Decentralized INS/GNSS System With MEMS-Grade Inertial Sensors Using QR-Factorized CKF

Hossein Nourmohammadi and Jafar Keighobadi

Abstract—Special approaches are required for integration of global navigation satellite system (GNSS) with a strap-down inertial navigation system (INS), particularly based on lowcost micro-electro mechanical system (MEMS)-grade inertial sensors. The proposed approach should be computationally efficient, mathematically nonsingular, and executable on small digital signal processor (DSP) modules. This paper presents a new INS/GNSS navigation system based on a direct decentralized integration scheme. Based on the proposed QR-factorized cubature Kalman filter (CKF) structure, two cascade filters are implemented for separate estimation of the orientation attitude-heading angles and the 3-D position/velocity components. Owing to the QR-factorization, the numerical errors in the update process of estimation covariance matrix are removed. Considering the nonlinear dynamics of the strap-down INS as well as the large uncertainties included in stochastic model of the MEMS-grade inertial sensors, the QR-factorized CKF yields enhanced accuracy and reliability compared with the pure Kalman filter. The decentralized integration scheme provides the separate estimation of orientation components from the position and velocity vectors. Therefore, the propagation of the position and velocity estimation errors into the orientation filter section does not occur. The performance of the presented system is assessed through real data of vehicular field tests.

Index Terms—Low-cost navigation, INS/GNSS system, MEMS-grade inertial sensors, integration scheme, QR-factorized CKF.

I. Introduction

ICRO-ELECTRO mechanical-system (MEMS)-grade accelerometers and gyroscopes are inserted along 3-axis orthogonal frames to produce low-cost inertial measurement unit (IMU) required in inertial navigation systems (INSs). Nowadays, wide range applications of low-cost INS in aerial, ground, and marine vehicles motivate enhancement of navigation accuracy. In strap-down INS, through sequential integration of high frequency specific forces and angular rotation rates measured by MEMS accelerometers and gyroscopes, the orientation angles, position and velocity components are obtained in a predefined reference coordinate frame. Owing to high update rate of inertial

Manuscript received February 21, 2017; accepted April 3, 2017. Date of publication April 12, 2017; date of current version May 5, 2017. This work was supported by the Iran National Science Foundation under Grant 93031367. The associate editor coordinating the review of this paper and approving it for publication was Dr. E. H. Yang. (Corresponding author: Jafar Keighobadi.)

The authors are with the Mechanical Engineering Department, University of Tabriz, Tabriz 5166614766, Iran (e-mail: hnourmohammadi@tabrizu.ac.ir; keighobadi@tabrizu.ac.ir).

Digital Object Identifier 10.1109/JSEN.2017.2693246

measurements, up to 1000 Hz and its autonomous navigation data, the INS noisy data are combined with low rate data of a global navigation satellite system (GNSS) [1]. Therefore, the limitations of GNSS like low update rate (up to 5 Hz), signal blockage in indoor applications, near tall buildings and especially lack of orientation angles determination are removed. On the other hand, large long-term errors of MEMS-grade inertial sensors lead to time-increasing navigation errors in INS stand-alone operation [2]. Therefore, combination of the INS with a GNSS receiver, which updates accurate position and velocity information even at 1 Hz, results in better performance and reliability of the so-called integrated INS/GNSS system.

An integrated INS/GNSS uses optimal/suboptimal data fusion algorithms mostly known as filter, estimator, observer and so on in literature. For example, Farhan and Kenneth have developed an error model of INS as the base of the extended Kalman filter (EKF) estimation algorithm of the INS/GNSS mechanization [3]. As an enhanced estimation method for multi-sensor data fusion, adaptive Kalman filter was used to provide smooth and continuous navigation data in the intervals of GPS blockage [4]. Wei et al. proposed a quadratic EKF technique by considering the second-order terms of Taylor approximation of nonlinear INS dynamics in propagation of estimation covariance matrix [5]. Based on stochastic modeling of quantization and colored noises of inertial sensors, Han and Wang improved the estimation of inertial sensor's drift and thereby the navigation accuracy [6]. Musavi and Keighobadi proposed an adaptive fuzzy neuro-observer to enhance the performance of the integrated INS/GNSS positioning systems [7]. Artificial neural networks as approximation of nonlinear terms have been used in the integration filter of INS/GNSS systems [8]. However, realtime implementation considerations of INS/GNSS system limit practical usage of fuzzy/neural network-based methods.

INS/GNSS systems can be categorized according to the depth of integration between INS and GNSS [9]. Loosely coupled and tightly coupled integration are two basic and more common schemes of INS/GNSS integration [10], [11]. In the loosely coupled system shown in Fig. 1, two separate filters operate independently. The first filter inside the GNSS pack computes position and velocity vectors using GNSS raw measurements including pseudo-range and deltarange or Doppler measurements including phase and frequency shift. The second external INS/GNSS filter estimates position,

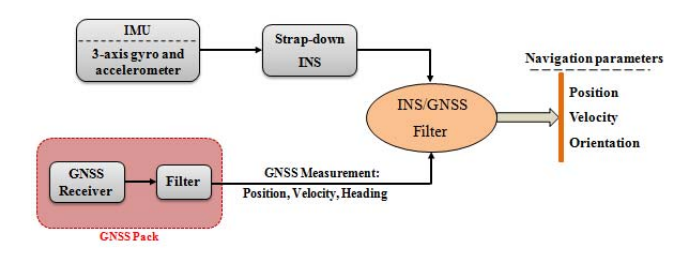


Fig. 1. Loosely coupled scheme for INS/GNSS integration.



Fig. 2. Tightly coupled scheme for INS/GNSS integration.

velocity, and attitude-heading angles by simultaneous using IMU measurements and GNSS position and velocity vectors in which the INS errors are compensated by GNSS. In the tightly coupled integration shown in Fig. 2, the INS navigation data and the GNSS raw measurements are optimally processed in a unique central filter and thus the separate filter of GNSS in the loosely coupled scheme is removed.

As the main advantage, using two separate filters in the loosely coupled scheme leads to the benefit of getting a smaller and simpler filter compared to the corresponding central filter of the tightly coupled scheme. Nowadays, the GNSS receivers with capable use of all available data of GPS, GLONASS, GALILEO, BEIDOU, and so on attenuate the weakness of loosely coupled integration of using partial available satellites.

Concerning with the loosely coupled integration of MEMS INS and GNSS, the current paper proposes a new integration technique as direct decentralized INS/GNSS. Direct implies that the basic nonlinear dynamics of the INS is incorporated in the estimation algorithm unlike the linearized INS model used in common research works in literature. Therefore, the incorporation of model linearization errors in propagation of the so-called time-update and measurement-update covariance matrices of estimation errors and consequently in the filter gain matrix is removed. The proposed nonlinear filter of INS/GNSS is designed as a QR-factorized cubature Kalman filter (CKF). Unlike the traditional EKF, the QR-factorized CKF does not need to compute the Jacobian matrices in which the firstorder linearization errors may lead to large errors in statistical mean and covariance of the state vector [12]. Furthermore, the QR-factorization method enhances the numerical stability and accuracy of the basic CKF.

The proposed integration technique is called decentralized since the orientation computation part is decoupled from the position and velocity estimation part. In classical INS/GNSS algorithms, the state estimation is carried out in a central filter. Obviously, any divergence in the position and velocity estimation propagation, for example due to low strength of GNSS signals, may lead to failure of the orientation update algorithm.

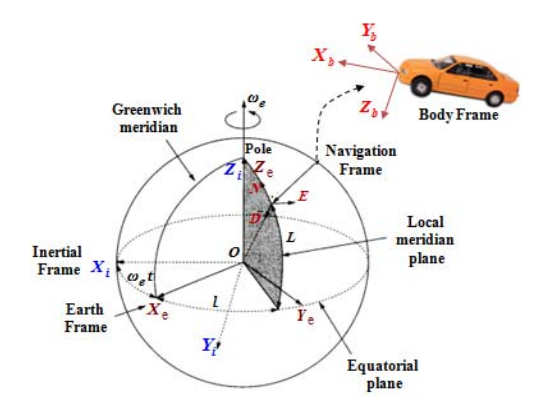


Fig. 3. Reference coordinate frames in the inertial navigation.

As a matter of fact, the decentralized integration method is considered in the paper to avoid broadcasting of the position and velocity estimation error into the orientation estimation. Through injection of attitude data obtained from gravity vector matching between body and reference frames, the estimation accuracy of orientation angles is enhanced. The orientation filter results are used in the position/velocity update filter based on cascade connection. In summary, the main contributions of the paper are:

- Design of a new integration technique as direct decentralized scheme to enhance the performance of the INSS/GNSS navigation system.
- Design of QR-factorized CKF to enhance the numerical stability and accuracy of the state estimation filter in INS/GNSS navigation system.

The performance of the proposed approach is assessed through vehicular field tests. Low-cost ADIS-16407 IMU is used as the MEMS-grade inertial sensors and the position and velocity measurements are provided by Garmin-35 GPS receiver. Highly accurate Vitans navigation system is used to produce the reference attitude data for evaluation

II. STRAP-DOWN INS DYNAMICS

The main reference frames also used in the paper are inertial i-frame, Earth e-frame, navigation n-frame and body b-frame of Fig. 3.

The n-frame is defined based on local level navigation frame with north-east-down (N-E-D) geodetic axes. Dynamic system of a strap-down INS includes three main parts as orientation dynamics, position dynamics, and velocity dynamics. In the current research work, owing to the minimal components and physical meaning, Euler angles are preferred to be used as orientation representation with respect to quaternion and direction cosine matrix (DCM). Euler angles represent the overall rotation of x-y-z b-frame with respect to NED n-frame. Based on z-y-x order in rotation sequence, Euler angles dynamics can be expressed as follows.

$$\dot{\varphi} = (\omega_y \sin \varphi + \omega_z \cos \varphi) \tan \theta + \omega_x$$

$$\dot{\theta} = \omega_y \cos \varphi - \omega_z \sin \varphi$$

$$\dot{\psi} = (\omega_y \sin \varphi + \omega_z \cos \varphi) \sec \theta$$
(1)

where, the orientation heading-pitch-roll angles shown as ψ , θ , and φ specify rotation components about z, y, and x

body axes, respectively. The angular rotation vector $\boldsymbol{\omega}_{nb}^b = [\omega_x \ \omega_y \ \omega_z]^T$ specifies the rotation rate of the b-frame with respect to the n-frame, projected in b-frame. $\boldsymbol{\omega}_{nb}^b$ is computed from gyroscopes measurement vector, $\boldsymbol{\omega}_{ib}^b$ as:

$$\boldsymbol{\omega}_{nb}^{b} = \boldsymbol{\omega}_{ib}^{b} - (\boldsymbol{\omega}_{ie}^{b} + \boldsymbol{\omega}_{en}^{b}) = \boldsymbol{\omega}_{ib}^{b} - \boldsymbol{C}_{n}^{b} [\boldsymbol{\omega}_{ie}^{n} + \boldsymbol{\omega}_{en}^{n}]$$
 (2)

where, ω_{ie}^n is the rotation rate vector of Earth expressed in the n-frame and ω_{en}^n is the rotation rate of n-frame with respect to e-frame known as the transportation rate of vehicle, too. The transformation/rotation matrix from b-frame to n-frame known as DCM matrix is represented by C_h^n [13]:

$$C_b^a = \begin{bmatrix}
C\theta C\psi & -C\varphi S\psi + S\varphi S\theta C\psi & S\varphi S\psi + C\varphi S\theta C\psi \\
C\theta S\psi & C\varphi C\psi + S\varphi S\theta S\psi & -S\varphi C\psi + C\varphi S\theta S\psi \\
-S\theta & S\varphi C\theta & C\varphi C\theta
\end{bmatrix}$$
(3)

where, *C* and *S* stand for cosine and sine functions, respectively. Solution of (1) in the strap-down framework results in updated open-loop Euler angles of under-navigation vehicle whose longitudinal-lateral-vertical axes are aligned along the x-y-z axes of IMU b-frame.

Like GNSS, the INS position vector in spherical platform is characterized by latitude, L longitude, l and height, h with the following governing equations [14].

$$\dot{L} = \frac{v_N}{R_N + h}, \quad \dot{l} = \frac{v_E}{(R_E + h)\cos L}, \quad \dot{h} = -v_D$$
 (4)

where, the velocity vector components in the n-frame are considered as, $v^n = [v_N \ v_E \ v_D]^T$. R_N and R_E represent Earth meridian and transverse radii of curvature, respectively.

The velocity components of the strap-down INS in the n-frame are developed as follows [14].

$$\dot{v}_N = f_N - 2\omega_e v_E \sin L + \frac{v_N v_D}{R_N + h} - \frac{v_E^2 \tan L}{R_E + h} \tag{5}$$

$$\dot{v}_E = f_E + 2\omega_e(v_N \sin L + v_D \cos L) + \frac{v_E}{R_E + h} (v_D + v_N \sin L)$$
(6)

$$\dot{v}_D = f_D - 2\omega_e v_E \cos L - \frac{v_E^2}{R_E + h} + \frac{v_N^2}{R_N + h} + g \quad (7)$$

where, g and ω_e stand for the Earth gravity and rotation rate, respectively. The components of $f^n = [f_N \ f_E \ f_D]^T$ represent the specific force vector by accelerometers projected in the n-frame. Using (1) - (7), the navigation data can be updated continuously providing initial alignment values of navigation data and the IMU measurements. However, due to large uncertainties of MEMS sensors data, bias instability, and 3-order integrations imposed on the uncertainties, the navigation error of the stand-alone INS quickly increases over time. Therefore, for long-time applications, INS should be integrated with an auxiliary navigation system like a GNSS.

III. INS/GNSS INTEGRATED NAVIGATION SYSTEM

INS and GNSS have complementary characteristics which would be used in the integrated mode to cover disadvantages

of individual systems. However, the integration of INS and GNSS requires special software techniques in particular by use of low-cost inertial sensors. State estimation algorithm for data fusion and the integration mechanization are two key steps in developing an INS/GNSS system. This section explains the paper contributions concerning these two aspects.

A. State Estimation Algorithm

Among optimal state estimation algorithms, EKF is probably the most widely used algorithm in nonlinear systems like integrated navigation systems. As the nonlinear extension of standard Kalman filter, EKF suffers from some drawbacks mainly arise from its linearization-based structure. For example, EKF has difficulties in implementation, tuning, and is reliable only for systems which remain almost linear on the time scale of the system updates [15]. Moreover, in nonlinear systems which are not differentiable, linearization may lead to large errors in mean and covariance of estimations. Cumbersome operation in derivation of the Jacobian matrices motivates the design of more efficient nonlinear filters. The unscented Kalman filter (UKF) and the CKF are two alternatives to the EKF. The UKF uses unscented transformation in which the Gaussian distribution is represented by a set of deterministically chosen sigma points. The CKF is based on third-degree spherical-radial cubature rule for numerical computation of Gaussian-weighted multi-dimensional integrals appearing in Bayesian filter. A set point called cubature points are used in the CKF to numerically compute the integrals [16]. As the main difference between UKF and CKF, the sigma points contain one more point in its center with a tuning parameter, κ . The center point is highly significant as it carries more weight which is commonly negative for highdimensional systems. For systems of dimension more than 3, the negative weight of the center sigma point may lead to non-positive semi-definite covariance matrix which means the failure of filter. Compared with the UKF troubles, the CKF enhances the numerical stability property in high-dimensional filtering problems [17].

According to the above-mentioned explanations, the CKF algorithm is preferred for state estimation in the proposed MEMS INS/GNSS system. Furthermore, the CKF is modified by use of QR-factorization method to achieve a better accuracy and numerical stability of navigation algorithm.

B. QR-Factorized CKF

Consider the following discrete-time nonlinear dynamics system.

$$\mathbf{x}_{k} = \mathbf{f}(\mathbf{x}_{k-1}, \mathbf{u}_{k-1}) + \mathbf{v}_{k-1}$$

$$\mathbf{y}_{k} = \mathbf{h}(\mathbf{x}_{k}, \mathbf{u}_{k}) + \mathbf{w}_{k}$$
 (8)

where, $\mathbf{x}_k \in \mathbb{R}^n$, $\mathbf{u}_k \in \mathbb{R}^r$, and $\mathbf{y}_k \in \mathbb{R}^m$ show the state, input, and output vectors; $\mathbf{f}(\cdot)$ and $\mathbf{h}(\cdot)$ are nonlinear dynamics and measurement vectors; \mathbf{v}_k and \mathbf{w}_k show the process and measurement noises of covariance \mathbf{Q}_k and \mathbf{R}_k .

CKF was first proposed by Arasaratnam and a comprehensive discussion was presented in [18]. Here, the CKF algorithm is summarized in the following steps.

Step1. Initialization

The estimated state vector and covariance matrix of estimation error are initialized as:

$$\hat{\mathbf{x}}_{0|0} = \mathbb{E}(\mathbf{x}_{0|0})
\mathbf{P}_{0|0} = \mathbb{E}[(\mathbf{x}_{0|0} - \hat{\mathbf{x}}_{0|0})(\mathbf{x}_{0|0} - \hat{\mathbf{x}}_{0|0})^T]$$
(9)

Step2. Time update

The cubature points are generated for i = 1, 2, ..., 2n.

$$\mathbf{X}_{i,k-1|k-1} = \mathbf{S}_{k-1|k-1} \boldsymbol{\zeta}_i + \hat{\mathbf{x}}_{k-1|k-1}$$
 (10)

where, $\mathbf{S}_{k-1|k-1}$ is the square root of covariance matrix, $\mathbf{P}_{k-1|k-1}$ whereas $\mathbf{S}_{k-1|k-1}\mathbf{S}_{k-1|k-1}^T = \mathbf{P}_{k-1|k-1}$. Also, $\boldsymbol{\zeta}_i$ is the i^{th} column of the matrix $\sqrt{n}\left[\mathbf{I}_{n\times n} - \mathbf{I}_{n\times n}\right]$ in which, I stands for identity matrix.

Now, the propagated cubature points are computed as:

$$\mathbf{X}_{i,k|k-1}^* = \mathbf{f}\left(\mathbf{X}_{i,k-1|k-1}, \mathbf{u}_{k-1}\right)$$
 (11)

The predicted state and covariance matrix are computed as:

$$\hat{\mathbf{x}}_{k|k-1} = \frac{1}{2n} \sum_{i=1}^{2n} \mathbf{X}_{i,k|k-1}^*$$
 (12)

$$\mathbf{P}_{k|k-1} = \frac{1}{2n} \sum_{i=1}^{2n} \mathbf{X}_{i,k|k-1}^* \mathbf{X}_{i,k|k-1}^{*T} - \hat{\mathbf{x}}_{k|k-1} \hat{\mathbf{x}}_{k|k-1}^{T} + \mathbf{Q}_{k-1}$$

Step3. Measurement update

The cubature points are generated for i = 1, 2, ..., 2n.

$$\mathbf{X}_{i,k|k-1} = \mathbf{S}_{k|k-1} \boldsymbol{\zeta}_i + \hat{\mathbf{x}}_{k|k-1} \tag{14}$$

Based on the propagated cubature points for i = 1, 2, ..., 2nas:

$$\mathbf{Y}_{i|k|k-1} = \mathbf{h} \left(\mathbf{X}_{i|k|k-1}, \mathbf{u}_k \right) \tag{15}$$

the predicted measurements are obtained as follows.

$$\hat{\mathbf{y}}_{k|k-1} = \frac{1}{2n} \sum_{i=1}^{2n} \mathbf{Y}_{i,k|k-1}$$
 (16)

Now, the innovation covariance and the cross-covariance matrices are updated.

$$\mathbf{P}_{y,k|k-1} = \frac{1}{2n} \sum_{i=1}^{2n} \mathbf{Y}_{i,k|k-1} \, \mathbf{Y}_{i,k|k-1}^T - \hat{\mathbf{y}}_{k|k-1} \, \hat{\mathbf{y}}_{k|k-1}^T + \mathbf{R}_k$$

$$\mathbf{P}_{xy,k|k-1} = \frac{1}{2n} \sum_{i=1}^{2n} \mathbf{X}_{i,k|k-1} \ \mathbf{Y}_{i,k|k-1}^T - \hat{\mathbf{x}}_{k|k-1} \ \hat{\mathbf{y}}_{k|k-1}^T$$
(18)

The cubature Kalman gain is obtained as:

$$\mathbf{K}_k = \mathbf{P}_{xy,k|k-1} \, \mathbf{P}_{y,k|k-1}^{-1} \tag{19}$$

The measurement-update of state vector and covariance matrix are computed as the final step.

$$\hat{\mathbf{x}}_{k|k} = \hat{\mathbf{x}}_{k|k-1} + \mathbf{K}_k (\mathbf{y}_k - \hat{\mathbf{y}}_{k|k-1})$$
 (20)

$$\mathbf{P}_{k|k} = \mathbf{P}_{k|k-1} - \mathbf{K}_k \, \mathbf{P}_{v|k|k-1} \, \mathbf{K}_k^T \tag{21}$$

Symmetry and positive definiteness are two basic properties of a covariance matrix. Since the square root of estimation error covariance matrix of CKF is required to generate the cubature points, numerical computation errors affecting the positive definiteness of the covariance matrix could stop the execution of CKF algorithm. As an important solution, a modified CKF is proposed in which the computation of square root of covariance matrix is removed. In order to acquire this purpose, all the covariance matrices of the CKF algorithm should be reformulated. Distribution of the cubature points $(\mathbf{X}_{i|k|k-1}^*)$ over the predicted state $(\hat{\mathbf{x}}_{k|k-1})$ is defined

$$\hat{\boldsymbol{e}}_{i,\mathbf{x}}^* = \mathbf{X}_{i,k|k-1}^* - \hat{\mathbf{x}}_{k|k-1}$$
 (22)

Accordingly, the following weighted-centered matrix is con-

$$\chi_{k|k-1}^* = \frac{1}{\sqrt{2n}} \left[\hat{e}_{1,x}^* \ \hat{e}_{2,x}^* \dots \ \hat{e}_{2n,x}^* \right]$$
 (23)

Now, the covariance of prediction error is redefined as:

$$\mathbf{P}_{k|k-1} = \begin{bmatrix} \mathbf{\chi}_{k|k-1}^* & \mathbf{S}_{\mathbf{Q}_{k-1}} \end{bmatrix} \begin{bmatrix} \mathbf{\chi}_{k|k-1}^* & \mathbf{S}_{\mathbf{Q}_{k-1}} \end{bmatrix}^T$$
(24)

where, $S_{Q_{k-1}}$ denotes the square root of Q_{k-1} . Similarly, the following innovation covariance and the cross-covariance matrices are developed as:

$$\mathbf{P}_{y,k|k-1} = \begin{bmatrix} \mathbf{\Upsilon}_{k|k-1} & \mathbf{S}_{\mathbf{R}_k} \end{bmatrix} \begin{bmatrix} \mathbf{\Upsilon}_{k|k-1} & \mathbf{S}_{\mathbf{R}_k} \end{bmatrix}^T$$
 (25)

$$\mathbf{P}_{xv,k|k-1} = \mathbf{\chi}_{k|k-1} \mathbf{\Upsilon}_{k|k-1}^T \tag{26}$$

where, $S_{\mathbf{R}_k}$ denotes the square root of \mathbf{R}_k and $\Upsilon_{k|k-1}$ is obtained as:

$$\Upsilon_{k|k-1} = \frac{1}{\sqrt{2n}} \left[\hat{e}_{1,y} \hat{e}_{2,y} ... \hat{e}_{2n,y} \right]$$
 (27)

$$\hat{\boldsymbol{e}}_{i,y} = \mathbf{Y}_{i,k|k-1} - \hat{\mathbf{y}}_{k|k-1} \tag{28}$$

Furthermore, the updated error covariance, $P_{k|k}$ is reformulated based on the following procedure. Rearranging (19) and (21) results in:

$$\mathbf{P}_{k|k} = \mathbf{P}_{k|k-1} - \mathbf{P}_{xy|k|k-1} \mathbf{K}_k^T \tag{29}$$

$$\mathbf{P}_{k|k} = \mathbf{P}_{k|k-1} - \mathbf{P}_{xy,k|k-1} \mathbf{K}_k^T$$

$$\mathbf{K}_k \mathbf{P}_{xy,k|k-1}^T = \mathbf{K}_k \mathbf{P}_{y,k|k-1} \mathbf{K}_k^T$$
(29)

Aggregating (29) and (30) yields:

$$\mathbf{P}_{k|k} = \mathbf{P}_{k|k-1} - \mathbf{P}_{xy,k|k-1} \mathbf{K}_k^T + \mathbf{K}_k \mathbf{P}_{y,k|k-1} \mathbf{K}_k^T - \mathbf{K}_k \mathbf{P}_{xy,k|k-1}^T$$
(31)

Using the fact that $\mathbf{P}_{k|k-1} = \mathbf{\chi}_{k|k-1} \mathbf{\chi}_{k|k-1}^T$, and also replacing (25) and (26) into (31) results in:

$$\mathbf{P}_{k|k} = \mathbf{\chi}_{k|k-1} \mathbf{\chi}_{k|k-1}^{T} - \mathbf{\chi}_{k|k-1} \mathbf{\Upsilon}_{k|k-1}^{T} \mathbf{K}_{k}^{T} + \mathbf{K}_{k} (\mathbf{\Upsilon}_{k|k-1} \mathbf{\Upsilon}_{k|k-1}^{T} + \mathbf{S}_{\mathbf{R}_{k}} \mathbf{S}_{\mathbf{R}_{k}}^{T}) \mathbf{K}_{k}^{T} - \mathbf{K}_{k} \mathbf{\Upsilon}_{k|k-1} \mathbf{\chi}_{k|k-1}^{T}$$

$$(32)$$

Equation (32) can be rearranged as follows:

$$\mathbf{P}_{k|k} = \begin{bmatrix} \mathbf{\chi}_{k|k-1} - \mathbf{K}_k \mathbf{\Upsilon}_{k|k-1} & \mathbf{K}_k \mathbf{S}_{\mathbf{R}_k} \end{bmatrix} \\ \begin{bmatrix} \mathbf{\chi}_{k|k-1} - \mathbf{K}_k \mathbf{\Upsilon}_{k|k-1} & \mathbf{K}_k \mathbf{S}_{\mathbf{R}_k} \end{bmatrix}^T$$
(33)

Therefore, all of the covariance matrices appearing in the CKF may be written in the factorized form as, $P = SS^{T}$. The matrix, S can be simply considered as the square root of P. Furthermore, by decrease of computational burden, a triangularization process on matrices will lead to more efficient results. Here, a QR-factorization algorithm is applied to compute S. In QR-factorization, a matrix S is decomposed into product of two matrices as, S = QR in which, Q is an orthogonal matrix and R is an upper triangular matrix [19]. Based on the QR-factorization of S^T , the covariance matrix is factorized as:

$$\mathbf{P} = \mathbf{S}\mathbf{S}^T = \mathbf{R}^T \mathbf{O}^T \mathbf{O} \mathbf{R} = \mathbf{R}^T \mathbf{R}$$
 (34)

Therefore, we obtain $S = \mathbb{R}^T$. Based on orthogonality of \mathbb{Q} according to (34), the square root of covariance can be computed as upper triangular matrix, \mathbb{R} . By triangular matrix, \mathbb{S} , the efficient computational burden of newly developed filter of INS/GNSS will require less memory storage together with low-cost small microprocessor board.

The proposed QR-factorization algorithm can now be applied on the predicted error covariance matrix (24), the innovation covariance matrix (25), and the updated covariance matrix (33). Therefore, the proposed QR-factorized CKF algorithm is developed with the following summarized steps.

Step 1. Initialization

The estimated state vector and covariance matrix of estimation error vector are initialized, respectively as:

$$\hat{\mathbf{x}}_{0|0} = \mathbb{E}(\mathbf{x}_{0|0})
\mathbf{P}_{0|0} = \mathbb{E}[(\mathbf{x}_{0|0} - \hat{\mathbf{x}}_{0|0})(\mathbf{x}_{0|0} - \hat{\mathbf{x}}_{0|0})^T]$$
(35)

Note that since as a design parameter $P_{0|0}$ is given as a diagonal matrix, $S_{0|0}$ is easily computed.

Step2. Time update

The cubature points are generated for i = 1, 2, ..., 2n:

$$\mathbf{X}_{i,k-1|k-1} = \mathbf{S}_{k-1|k-1} \, \boldsymbol{\zeta}_i + \hat{\mathbf{x}}_{k-1|k-1} \tag{36}$$

The propagated cubature points are computed as:

$$\mathbf{X}_{i,k|k-1}^* = \mathbf{f} \left(\mathbf{X}_{i,k-1|k-1}, \ \mathbf{u}_{k-1} \right)$$
 (37)

The predicted state is computed as:

$$\hat{\mathbf{x}}_{k|k-1} = \frac{1}{2n} \sum_{i=1}^{2n} \mathbf{X}_{i,k|k-1}^*$$
 (38)

The square root of the predicted error covariance is calculated based on (22) through (24).

$$\mathbf{S}_{k|k-1} = \left(\operatorname{qr} \left(\left[\mathbf{\chi}_{k|k-1}^* \; \mathbf{S}_{\mathbf{Q}_{k-1}} \right] \right)^T \right)^T \tag{39}$$

where, $qr(\cdot)$ denotes the QR-factorization function.

Step3. Measurement update

The cubature points are generated for i = 1, 2, ..., 2n:

$$\mathbf{X}_{i,k|k-1} = \mathbf{S}_{k|k-1} \, \boldsymbol{\zeta}_i + \hat{\mathbf{x}}_{k|k-1} \tag{40}$$

Based on the propagated cubature points for i = 1, 2, ..., 2n as:

$$\mathbf{Y}_{i,k|k-1} = \mathbf{h} \left(\mathbf{X}_{i,k|k-1}, \mathbf{u}_k \right) \tag{41}$$

the predicted measurements are obtained as follows.

$$\hat{\mathbf{y}}_{k|k-1} = \frac{1}{2n} \sum_{i=1}^{2n} \mathbf{Y}_{i,k|k-1}$$
 (42)

The square root of the innovation covariance matrix is computed based on (25), (27), and (28) as:

$$\mathbf{S}_{y,k|k-1} = \left(\operatorname{qr} \left(\left[\mathbf{\Upsilon}_{k|k-1} \ \mathbf{S}_{\mathbf{R}_k} \right] \right)^T \right)^T \tag{43}$$

The cross-covariance matrix is computed as:

$$\mathbf{P}_{xy,\,k|k-1} = \mathbf{\chi}_{k|k-1} \mathbf{\Upsilon}_{k|k-1}^{T} \tag{44}$$

where, $\chi_{k|k-1}$ is computed as follows.

$$\chi_{k|k-1} = \frac{1}{\sqrt{2n}} \left[\hat{e}_{1,\mathbf{x}} \hat{e}_{2,\mathbf{x}} ... \hat{e}_{2n,\mathbf{x}} \right]$$
(45)

$$\hat{\boldsymbol{e}}_{i,\mathbf{x}} = \mathbf{X}_{i,k|k-1} - \hat{\mathbf{x}}_{k|k-1} \tag{46}$$

The square root cubature Kalman gain is obtained as:

$$\mathbf{K}_{k} = \left(\mathbf{P}_{xy,k|k-1} / \mathbf{S}_{y,k|k-1}^{T}\right) / \mathbf{S}_{y,k|k-1}$$

$$\tag{47}$$

The measurement-update of state vector is performed as:

$$\hat{\mathbf{x}}_{k|k} = \hat{\mathbf{x}}_{k|k-1} + \mathbf{K}_k(\mathbf{y}_k - \hat{\mathbf{y}}_{k|k-1})$$
 (48)

Finally, the square root of the updated error covariance matrix is obtained based on (33):

$$\mathbf{S}_{k|k} = \left(\operatorname{qr} \left(\left[\mathbf{\chi}_{k|k-1} - \mathbf{W}_k \mathbf{\Upsilon}_{k|k-1} \ \mathbf{W}_k \mathbf{S}_{\mathbf{R}_k} \right] \right)^T \right)^T \tag{49}$$

As the main specification, the QR-factorized CKF explicitly operates with the square root decomposition of the covariance matrices which in turn results in improved numerical stability and accuracy of the estimation algorithm. The superiority of the QR-factorized CKF with respect to the pure CKF is particularly significant in low-cost INS/GNSS systems. Owing to large uncertainty and limited accuracy of MEMS-grade inertial sensors, the covariance matrix is more likely to be non-positive definite. Consequently, compared with the CKF, the QR-factorized CKF yields correct and optimal estimations even in the presence of undesirable inaccuracies.

C. Integration Mechanization

In this section, the applied mechanization of integration between the strap-down INS and the GNSS is described. The subject is to develop a reliable INS/GNSS navigation system even though low-cost MEMS sensors are used in IMU. As shown in Fig. 4, a direct decentralized integration scheme is designed for the proposed INS/GNSS system. In the proposed scheme, the orientation filter is separated from the position/velocity filter. Hence, the estimation errors of position and velocity components are prevented to be propagated into the orientation computations. Fig. 4 shows that the connection between the orientation filter and the position/velocity filter is based on cascade connection mechanization. First, the attitude and heading angles are estimated in the orientation filter algorithm. Following, feeding of updated angles into the velocity dynamics of the strap-down INS, the position vector

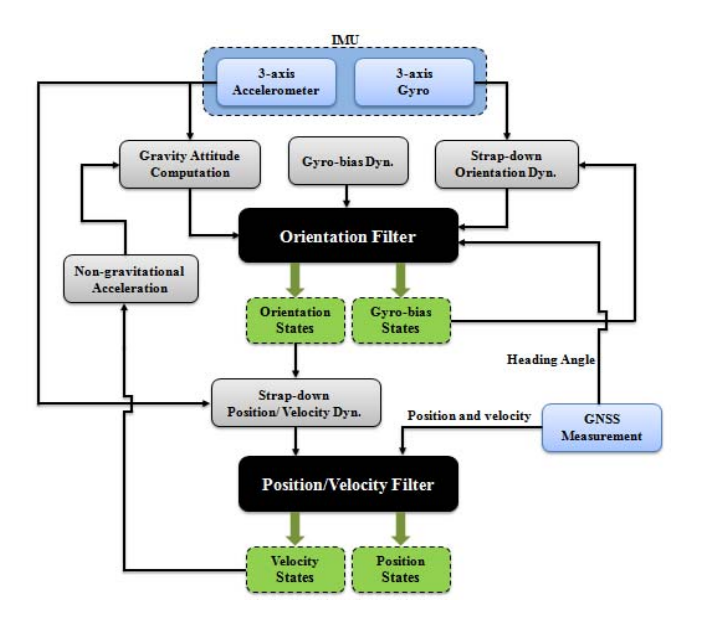


Fig. 4. Direct decentralized integration scheme for INS/GNSS system.

and velocity vector components are updated in the second separate filter.

Euler angles configuration has been considered in the orientation determination section of the designed INS/GNSS. Therefore, the dynamics system of the orientation filter uses a six states vector comprising the roll, pitch, and yaw angles as well as gyroscopes drift components along body x-y-z axes. Adding drift components of gyroscopes in (1) results in the following completed dynamics of orientation angles.

$$\dot{\varphi} = ((\omega_y - D_y)\sin\varphi + (\omega_z - D_z)\cos\varphi)\tan\theta + \omega_x - D_x$$

$$\dot{\theta} = (\omega_y - D_y)\cos\varphi - (\omega_z - D_z)\sin\varphi$$

$$\dot{\psi} = ((\omega_y - D_y)\sin\varphi + (\omega_z - D_z)\cos\varphi)\sec\theta$$
(50)

where, D_x , D_y and D_z stand for the drift components under the following Gauss-Markov dynamics.

$$\dot{D}_i = -\beta D_i + \sigma \sqrt{2\beta} w(t), \quad i = x, y, z$$
 (51)

where, β and σ are the correlation coefficient and the standard deviation of the sensor measurement and w(t) represents Gaussian white noise. For the orientation filter, the measurement vector is constructed by use of the gravity matched attitude angles and the GNSS heading angle.

$$\mathbf{Z}_1 = \begin{bmatrix} \varphi^{acc} & \theta^{acc} & \psi^G \end{bmatrix}^T \tag{52}$$

where, φ^{acc} and θ^{acc} are the roll and pitch angles through the gravity matching, respectively and ψ^G is the GNSS-based heading angle. The matching between the accelerometersensed gravity and the reference gravity vector yields [20]:

$$\begin{bmatrix} f_x^b \\ f_y^b \\ f_z^b \end{bmatrix} = \begin{bmatrix} C_n^b \end{bmatrix} \begin{bmatrix} 0 \\ 0 \\ -g \end{bmatrix}$$
 (53)

The gravity vector matching (53) is normalized as follows.

$$\frac{1}{norm(\mathbf{f}^b)} \begin{bmatrix} f_x^b \\ f_y^b \\ f_z^b \end{bmatrix} = \begin{bmatrix} C_n^b \end{bmatrix} \begin{bmatrix} 0 \\ 0 \\ -1 \end{bmatrix}$$
 (54)



Fig. 5. Vehicular field test and navigation hardware.

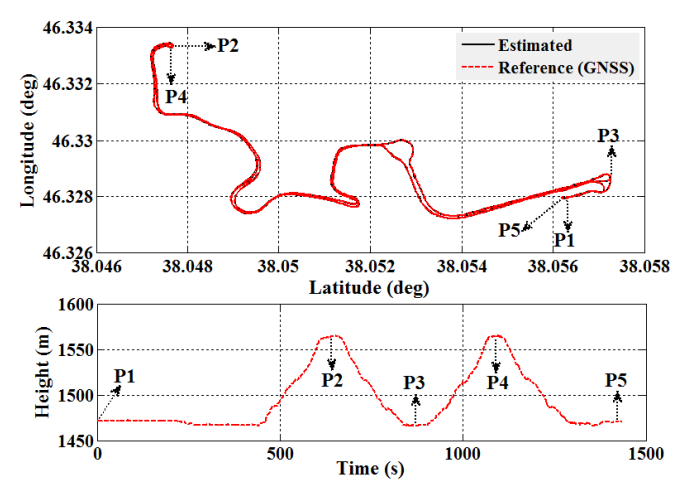


Fig. 6. Estimated and reference geographical latitude-longitude trajectory and height trajectory during test #1.

Now, the gravity attitude angles can be obtained by use of (3) and (54):

$$\varphi^{acc} = a \tan 2 \left(-f_y^b, -f_z^b \right), \quad \theta^{acc} = a \sin \left(\frac{f_x^b}{norm(f^b)} \right)$$
(55)

where, atan2 and asin represent the four-quadrant version of the arctangent and the arcsine, respectively. However, (55) remains accurate during non-accelerated maneuvers of the under-navigation vehicle. When the vehicle undergoes non-gravitational acceleration for example in dynamical maneuvers, considerable errors may be produced by (55). Therefore, the non-gravitational acceleration terms should be removed in computation of attitude angles from the accelerometer measurements. Using the fact that the non-gravitational acceleration of a car vehicle is mainly produced along its longitudinal axes aligned with the body x-axis, the accelerometer-sensed gravity term is approximated as follows.

$$(f_x^b)_g = f_x^b - sign\left(norm(\mathbf{f}^b) - norm(\mathbf{f}_0^b)\right)norm(\dot{\mathbf{v}}^n)$$
(56)

(54) where, f_0^b denotes the specific force measured by the accelerometer in a stationary mode. Accordingly, the gravity

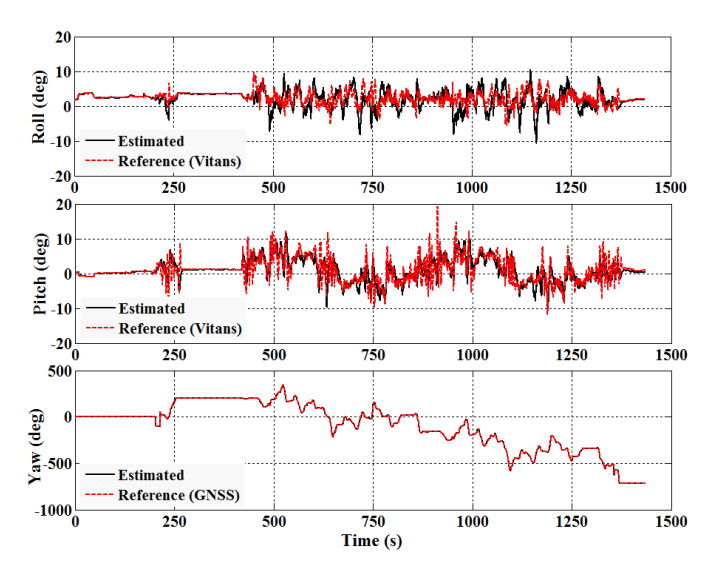


Fig. 7. Estimated orientation angles compared to Vitans attitude angle and GNSS heading during test #1.

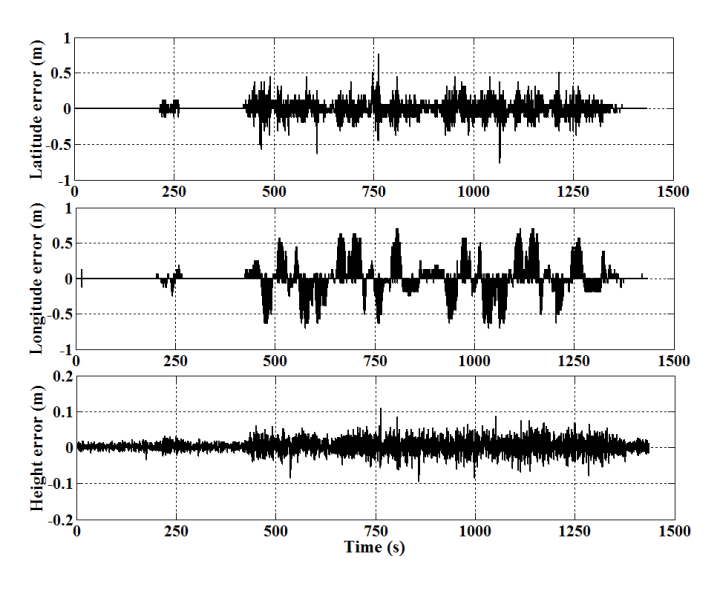


Fig. 8. Estimation error of the position states in test #1.

pitch angle in (55) is corrected as:

$$\theta^{acc} = a \sin\left(\frac{(f_x^b)_g}{norm(f_0^b)}\right)$$
 (57)

Now, the QR-factorized CKF is imposed on the dynamics system of (50) and (51) and the measurement of (52) and the orientation filter configuration is completed. Hereby, the QR-factorized CKF orientation filter could optimally attenuate the remaining uncertainties in the dynamics system and measurement equations.

Next, the configuration of position/velocity filter is completed by implementation of the QR-factorized CKF on the dynamics system of (4) - (7) and the following measurement vector by GNSS receiver.

$$\mathbf{Z}_2 = \begin{bmatrix} L^G & l^G & h^G & v_N^G & v_E^G & v_D^G \end{bmatrix}$$
 (58)

where, for example, L^G shows the GNSS longitude. In the proposed integration scheme of INS/GNSS, the linearization

TABLE I
STATISTICAL PROPERTIES OF THE INERTIAL SENSOR IN ADIS-16407

Parameter	Gyro	Accelerometer
In-run bias stability (1σ)	0.007 deg/sec	0.2 mg
Random walk (1σ)	1.9 deg/√hr	0.2 m/sec/√hr
Output noise (no filtering)	0.8 deg/sec rms	9 mg rms

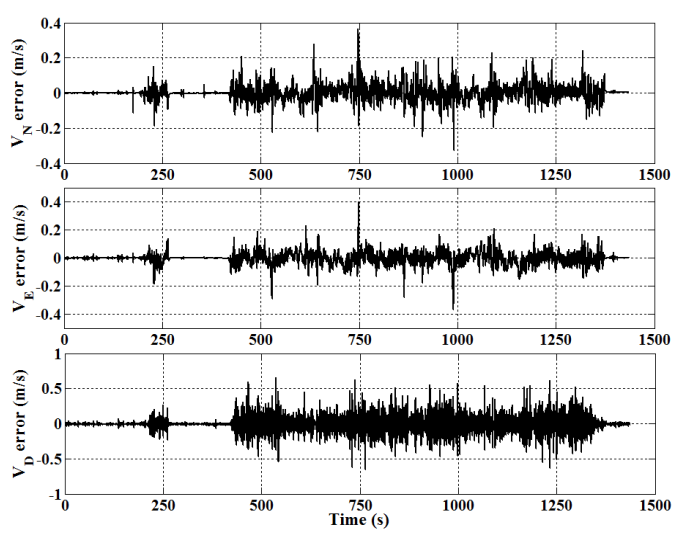


Fig. 9. Estimation error of the velocity states in test #1.

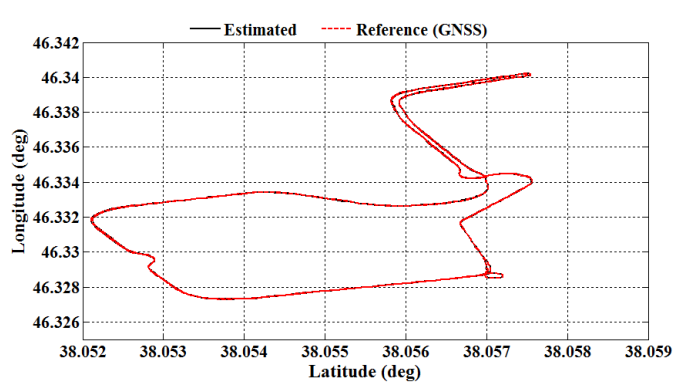


Fig. 10. Estimated and reference latitude-longitude trajectory in test #2.

of INS error model is removed by direct use of the nonlinear dynamics of strap-down INS in the estimation filter. Therefore, the estimation accuracy is not affected by the linearization error of the INS/GNSS system.

IV. EXPERIMENTAL RESULTS AND DISCUSSION

The proposed direct decentralized INS/GNSS system is evaluated in several vehicular field tests. The MEMS-grade inertial sensors of low-cost ADIS-16407 IMU are used to generate inertial data comprising of angular rates and specific forces. The main statistical properties of the inertial sensors in ADIS-16407 IMU are given in Table 1 [21].

The IMU was installed beside a precise Vitans navigation system, as shown in Fig. 5. Vitans system was developed by Teknol. Ltd, as a high-performance integrated navigation

Navigation	Direct decentralized scheme with QR-factorized CKF		Intelligent scheme with Adaptive fuzzy neuro-observer		Conventional integration with EKF	
parameter	Mean value of estimation error	Standard deviation of estimation error (±1σ)	Mean value of estimation error	Standard deviation of estimation error (±1σ)	Mean value of estimation error	Standard deviation of estimation error $(\pm 1 \sigma)$
Latitude (m)	0.00224	0.06437	-0.01435	1.1800	-0.11680	1.5540
Longitude (m)	0.00080	0.04358	0.03518	1.1690	-0.17550	1.9520
Height (m)	0.00344	0.01452	-0.01729	0.4504	-1.13300	0.8728
V-north (m/s)	0.00215	0.04226	0.04504	0.5300	0.09224	0.9187

0.00713

-0.00463

TABLE II $Mean\ Value\ and\ Standard\ Deviation\ of\ the\ Estimation\ Error\ in\ the\ Test\ \#1$

 $TABLE\ III$ Mean Value and Standard Deviation of the Estimation Error in the Test #2

0.5570

0.1604

Navigation	Direct decentralized scheme with QR-factorized CKF		Intelligent scheme with Adaptive fuzzy neuro-observer		Conventional integration with EKF	
parameter	Mean value of estimation error	Standard deviation of estimation error $(\pm 1\sigma)$	Mean value of estimation error	Standard deviation of estimation error (±1σ)	Mean value of estimation error	Standard deviation of estimation error $(\pm 1\sigma)$
Latitude (m)	0.00024	0.08102	-0.00565	0.6602	0.11430	1.0980
Longitude (m)	-0.00011	0.05506	0.01953	0.8928	-0.02129	1.5340
Height (m)	0.00265	0.01637	-0.01058	0.3282	0.67650	0.6720
V-north (m/s)	-0.00263	0.03995	0.01379	0.4596	-0.05872	0.6441
V-east (m/s)	-0.00183	0.04247	0.02272	0.6578	-0.03624	0.8089
V-down (m/s)	-0.00557	0.07862	-0.00138	0.1657	0.09583	0.2323

system, specifically for land applications [22]. The highly accurate attitude data provided by Vitans system are considered as the reference values for the attitude accuracy assessment of the proposed approach. The raw IMU measurements are acquired at a sampling rate of 50 Hz. The INS orientation, velocity and position are delivered at the same rate, but corrected by the GNSS data at a rate of 1 Hz in the QR-factorized CKF.

V-east (m/s)

V-down (m/s)

-0.00177

-0.00570

0.04120

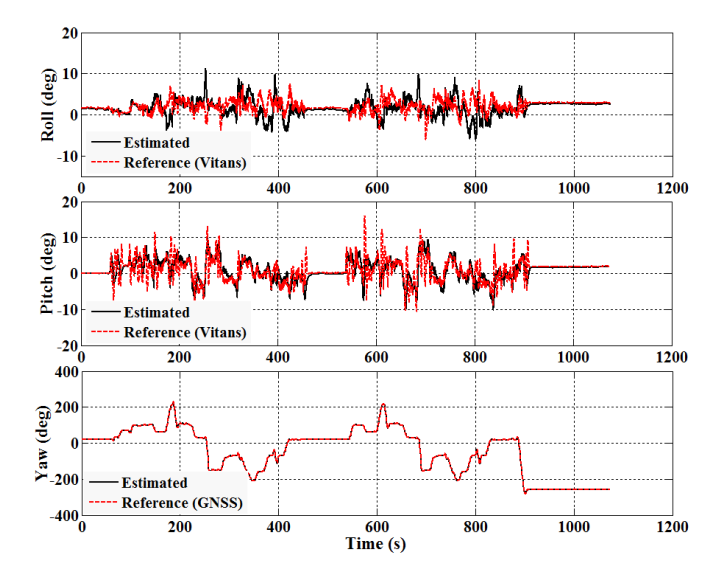
0.07260

The GNSS position and velocity measurements are provided by a set of Garmin-35 receiver and antenna in a single housing. As an important consideration, the GNSS antenna must have a clear view of the sky to provide a good coverage of GNSS satellites. Therefore, the test setup has been fixed on a rigid aluminum frame out of the vehicle body.

Three vehicular tests have been executed for experimental assessment of the proposed INS/GNSS system. Fig. 6 represents the vehicle trajectory during field test #1. The vehicle undergoes significant maneuvering in both the altitude and the heading angle (for example in the intervals 430-s to 620-s) along the uphill and downhill road trajectory.

Fig. 7 shows the performance of the proposed direct decentralized INS/GNSS algorithm in the orientation estimation compared to the attitude angles of Vitans system and the GNSS heading angle.

The estimation errors of the position and velocity components with respect to the reference GNSS data are shown in Figs. 8 and 9. For better evaluation of the QR-factorized CKF in the proposed direct decentralized INS/GNSS algorithm, the results are compared with those of two other algorithms including, conventional INS/GNSS system with EKF and intelligent INS/GNSS system with knowledge-based



0.14980

0.01498

1.3520

0.2163

Fig. 11. Estimated orientation states compared to Vitans attitude angle and GNSS heading during test #2.

approximators constructed by fuzzy logic and neural network methods. A comprehensive description of these algorithms was presented in [7]. To legitimize the comparisons, the mean value and the standard deviation of position and velocity estimation errors corresponding to each algorithm are accumulated in Table 2. The results clearly reveal that the proposed direct decentralized scheme with QR-factorized CKF results in superior position and velocity estimation in comparison to the intelligent scheme with adaptive fuzzy neuro-observer as well as the conventional integration with EKF algorithm.

Navigation	Direct decentralized scheme with QR-factorized CKF		Intelligent scheme with Adaptive fuzzy neuro-observer		Conventional integration with EKF	
parameter	Mean value of estimation error	Standard deviation of estimation error (±1σ)	Mean value of estimation error	Standard deviation of estimation error (±1σ)	Mean value of estimation error	Standard deviation of estimation error (±1σ)
Latitude (m)	-0.00555	0.06183	0.00961	1.1640	-0.12700	1.2720
Longitude (m)	0.00169	0.17360	0.04053	1.1540	0.24830	1.2980
Height (m)	-0.00483	0.02041	-0.07941	0.6633	-0.99710	0.7036
V-north (m/s)	0.00176	0.07896	-0.01613	0.5268	0.09349	0.7382
V-east (m/s)	0.00784	0.08274	-0.04840	0.5220	-0.19000	0.8414
V-down (m/s)	-0.00306	0.01373	-0.00330	0.1722	0.06543	0.2445

 ${\bf TABLE\ IV}$ Mean Value and Standard Deviation of the Estimation Error in the Test #3

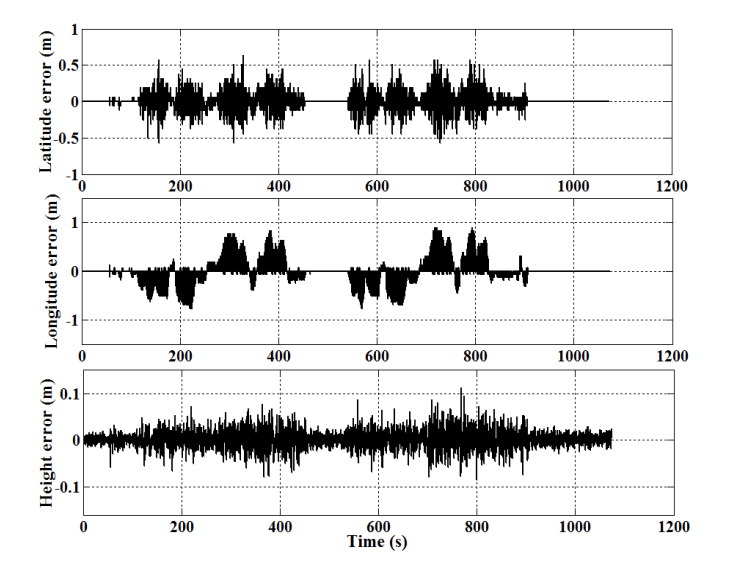


Fig. 12. Estimation error of the position states in test #2.

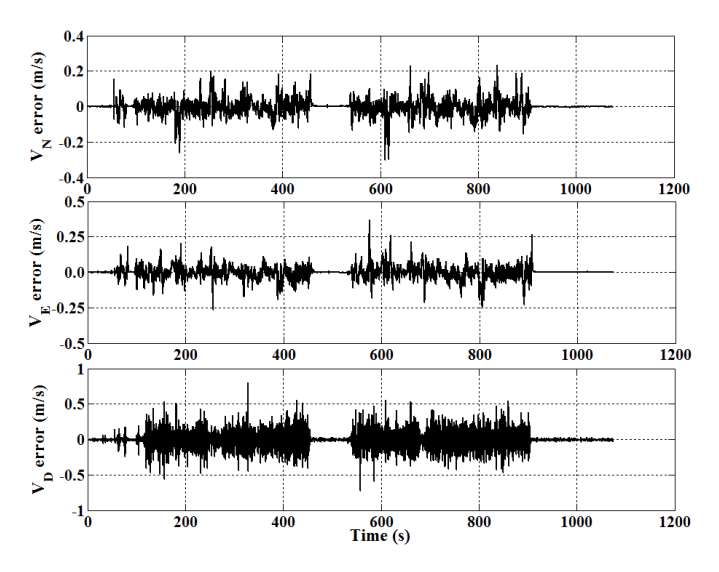


Fig. 13. Estimation error of the velocity states in test #2.

The second test has been executed for approximately 1100-s in a different urban area along a trajectory with wide range dynamics maneuvering, as shown in Fig. 10.

In Fig. 11, the estimated orientation angles in test #2 are compared with the attitude angles of the Vitans system and the

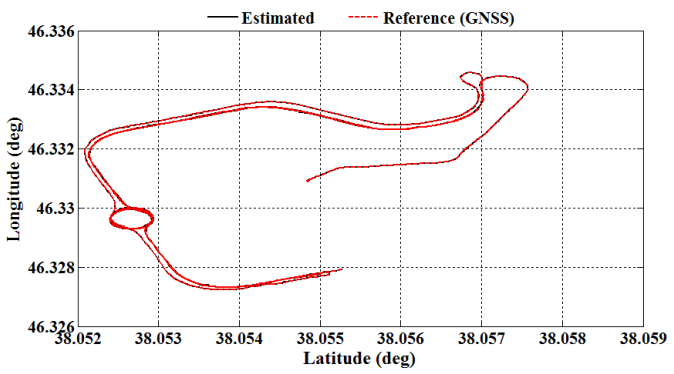


Fig. 14. Estimated and reference latitude-longitude trajectory in test #3.

GNSS heading angle. Figs. 12 and 13 show the position and velocity estimation error with respect to the reference values of the GNSS system in test #2.

Table 3 represents the statistical properties of the position and velocity estimation error during test # 2.

Furthermore, the proposed navigation algorithm has been evaluated in another vehicular test which takes approximately 700-s. Fig. 14 shows the estimated trajectory in the horizontal plane in comparison with the true reference trajectory during test #3. The mean value and the standard deviation of the position and velocity estimation error during test #3 are gathered in Table 4.

According to Figs 6, 10, and 14, the proposed algorithm guarantees perfect tracking along the test trajectory. Statistical analysis of the estimation error in Tables 2, 3, and 4 shows that the proposed algorithm significantly decreases the mean value and standard deviation of position and velocity estimation error.

V. CONCLUSIONS

In accordance with current global trends, specifically the demand to achieve the highest possible accuracy of navigation devices while simultaneously minimizing their costs, low-cost INS/GNSS systems have attracted much attention in many practical applications. Following these trends, we proposed a direct decentralized integration scheme for low-cost INS/GNSS navigation system. Toward this end, the QR-factorized CKF was designed and applied for the integration process of the proposed navigation system. Therefore, the numerical stability and accuracy of the estimation filters have

been improved. The proposed technique has been evaluated in several vehicular field tests. To legitimize the assessment, the results were analyzed in comparison with those of the intelligent scheme with adaptive fuzzy neuro-observer and the conventional INS/GNSS with EKF algorithm. Considering the statistical specifications of results gathered in Tables 2 through 4, the proposed direct decentralized integration with QR-factorized CKF decreases the mean value and the standard deviation of the position estimation error from 0.0258-m and 0.8513-m of the intelligent adaptive fuzzy neuro-observer and 0.4011-m and 1.2174-m of the conventional EKF to 0.0024-m and 0.0590-m, respectively. These data have been obtained by averaging the results of all three field tests. Furthermore, the mean and the standard deviation of the velocity estimation error from 0.0181-m/s and 0.4168-m/s in the intelligent algorithm and 0.0885-m/s and 0.6663-m/s in the EKF decreased to 0.0036-m/s and 0.0547-m/s by the proposed algorithm, respectively. Considering the navigation accuracy and the theoretical superiority of the proposed algorithm, it can provide more reliable performances, especially in low-cost INS/GNSS navigation systems.

REFERENCES

- [1] K. T. Leung, J. F. Whidborne, D. Purdy, and P. Barber, "Road vehicle state estimation using low-cost GPS/INS," *Mech. Syst. Signal Process.*, vol. 25, no. 6, pp. 1988–2004, Aug. 2011.
- [2] M. Zhong, J. Guo, and Z. Yang, "On real time performance evaluation of the inertial sensors for INS/GPS integrated systems," *IEEE Sensors J.*, vol. 16, no. 17, pp. 6652–6661, Sep. 2016.
- [3] F. A. Faruqi and K. J. Turner, "Extended Kalman filter synthesis for integrated global positioning/inertial navigation systems," *Appl. Math. Comput.*, vol. 115, nos. 2–3, pp. 213–227, Oct. 2000.
- [4] W. Bin, W. Jian, W. Jianping, and C. Baigen, "Study on adaptive GPS/INS integrated navigation system," in *Proc. IEEE Intell. Transp.* Syst., Oct. 2003, pp. 1016–1021.
- [5] W. Wang, Z.-Y. Liu, and R.-R. Xie, "Quadratic extended Kalman filter approach for GPS/INS integration," *Aerosp. Sci. Technol.*, vol. 10, no. 8, pp. 709–713, Dec. 2006.
- [6] S. Han and J. Wang, "Quantization and colored noises error modeling for inertial sensors for GPS/INS integration," *IEEE Sensors J.*, vol. 11, no. 6, pp. 1493–1503, Jun. 2011.
- [7] N. Musavi and J. Keighobadi, "Adaptive fuzzy neuro-observer applied to low cost INS/GPS," Appl. Soft Comput., vol. 29, pp. 82–94, Apr. 2015.
- [8] B. H. Kaygisiz, I. Erkmen, and A. M. Erkmen, "GPS/INS enhancement for land navigation using neural network," *J. Navigat.*, vol. 57, no. 2, pp. 297–310, May 2004.
- [9] S. Alban, D. M. Akos, S. M. Rock, and D. Gebre-Egziabher, "Performance analysis and architectures for INS-aided GPS tracking loops," in *Proc. Inst. Navigat. Nat. Tech. Meeting*, Jan. 2003, pp. 611–622.
- [10] v. Sokolović, G. Dikic, G. Markovic, R. Stancic, and N. Lukic, "INS/GPS navigation system based on MEMS technologies," *J. Mech. Eng.*, vol. 61, nos. 7–8, pp. 448–458, Jul. 2015.
- [11] G. Hu, S. Gao, and Y. Zhong, "A derivative UKF for tightly coupled INS/GPS integrated navigation," ISA Trans., vol. 56, pp. 135–144, May 2015.

- [12] D. Simon, Optimal State Estimation: Kalman, H Infinity, and Nonlinear Approaches. Hoboken, NJ, USA: Wiley, 2006.
- [13] P. Doostdar and J. Keighobadi, "Design and implementation of SMO for a nonlinear MIMO AHRS," *Mech. Syst. Signal Process.*, vol. 32, pp. 94–115, Oct. 2012.
- [14] D. Titterton and J. L. Weston, Strapdown Inertial Navigation Technology, vol. 17. Stevenage, U.K.: IET, 2004.
- [15] S. J. Julier and J. K. Uhlmann, "Unscented filtering and nonlinear estimation," *Proc. IEEE*, vol. 92, no. 3, pp. 401–422, Mar. 2004.
- [16] Y. Meng, S. Gao, Y. Zhong, G. Hu, and A. Subic, "Covariance matching based adaptive unscented Kalman filter for direct filtering in INS/GNSS integration," *Acta Astron.*, vol. 120, pp. 171–181, Mar./Apr. 2016.
- [17] L. Chang, B. Hu, A. Li, and F. Qin, "Transformed unscented Kalman filter," *IEEE Trans. Autom. Control*, vol. 58, no. 1, pp. 252–257, Jan. 2013.
- [18] I. Arasaratnam and S. Haykin, "Cubature Kalman filters," *IEEE Trans. Autom. Control*, vol. 54, no. 6, pp. 1254–1269, Jun. 2009.
- [19] L. N. Trefethen and D. I. Bau, *Numerical Linear Algebra*. Philadelphia, PA, USA: SIAM, 1997.
- [20] J. Keighobadi, "Fuzzy calibration of a magnetic compass for vehicular applications," *Mech. Syst. Signal Process.*, vol. 25, no. 6, pp. 1973–1987, Aug. 2011.
- [21] Analog Devices. (2011). Ten Degrees of Freedom Inertial Sensor. [Online]. Available: http://www.analog.com/media/en/technicaldocumentation/data-sheets/ADIS16407.pdf
- [22] Teknol. COMPANAV-2. (2012). [Online]. Available: http://www.teknol.ru/eng/pdf/CompaNav2T_eng.pdf



Hossein Nourmohammadi received the B.S. degree in mechanical engineering from the Nooshirvani University of Technology, Babol, Iran, in 2010, and the M.S. degree in mechanical engineering from the Amirkabir University of Technology (Tehran Polytechnic), Tehran, Iran, in 2012. He is currently pursuing the Ph.D. degree in mechanical engineering with the University of Tabriz, Iran. He has been a Research Assistant with the Navigation, Guidance and Control Laboratory, University of Tabriz, since 2013. His current research interests include

integrated navigation systems, estimation and identification, and nonlinear adaptive control.



Jafar Keighobadi received the B.S. degree in mechanical engineering from the University of Tabriz, Tabriz, Iran, in 1997, the M.S. and Ph.D. degrees in mechanical engineering and control systems from the Department of Mechanical Engineering, Amirkabir University of Technology (Tehran Polytechnic), Tehran, Iran, in 2000 and 2008, respectively. He joined the Faculty of Mechanical Engineering, University of Tabriz, as an Assistant Professor in 2008, where he is currently an Associate Professor with the Mechanical Engi-

neering Department. His research interests include artificial intelligence, estimation and identification, nonlinear robust control, and GNC.